



HAL
open science

Corynebacterium glutamicum pyruvate:quinone oxidoreductase: an enigmatic metabolic enzyme with unusual structural features

Cristiano da Silva Lameira, Sini Münßinger, Lu Yang, Bernhard Eikmanns,
Marco Bellinzoni

► **To cite this version:**

Cristiano da Silva Lameira, Sini Münßinger, Lu Yang, Bernhard Eikmanns, Marco Bellinzoni. Corynebacterium glutamicum pyruvate:quinone oxidoreductase: an enigmatic metabolic enzyme with unusual structural features. FEBS Journal, 2024, 291 (20), pp.4501-4521. 10.1111/febs.17232 . pasteur-04671083

HAL Id: pasteur-04671083

<https://pasteur.hal.science/pasteur-04671083v1>

Submitted on 13 Aug 2024






HAL is a multi-disciplinary open access archive for the deposit and dissemination of scientific research documents, whether they are published or not. The documents may come from teaching and research institutions in France or abroad, or from public or private research centers.

L'archive ouverte pluridisciplinaire **HAL**, est destinée au dépôt et à la diffusion de documents scientifiques de niveau recherche, publiés ou non, émanant des établissements d'enseignement et de recherche français ou étrangers, des laboratoires publics ou privés.



Distributed under a Creative Commons Attribution 4.0 International License

Corynebacterium glutamicum pyruvate:quinone oxidoreductase: an enigmatic metabolic enzyme with unusual structural features

Cristiano da Silva Lameira¹ , Sini Münßinger¹ , Lu Yang^{2,*} , Bernhard J. Eikmanns¹  and Marco Bellinzoni² 

¹ Institute of Molecular Biology and Biotechnology of Prokaryotes, University of Ulm, Germany

² Institut Pasteur, Université Paris Cité, CNRS UMR3528, Unité de Microbiologie Structurale, Paris, France

Keywords

carbon metabolism; *Corynebacterium glutamicum*; oxidative decarboxylation; pyruvate oxidase; pyruvate:quinone-oxidoreductase

Correspondence

B. J. Eikmanns, Institute of Molecular Biology and Biotechnology of Prokaryotes, University of Ulm, Albert-Einstein-Allee 11, 89081 Ulm, Germany
 Tel: 0049 731 5022707
 E-mail: bernhard.eikmanns@uni-ulm.de
 and

M. Bellinzoni, Institut Pasteur, Université Paris Cité, CNRS UMR3528, Unité de Microbiologie Structurale, F-75015 Paris, France
 Tel: 0033 1 45688608
 E-mail: marco.bellinzoni@pasteur.fr

Present address

Wuhan Institute of Biological Products Co. Ltd., China

(Received 2 April 2024, revised 12 June 2024, accepted 19 June 2024)

doi:10.1111/febs.17232

Pyruvate:quinone oxidoreductase (PQO) is a flavin-containing peripheral membrane enzyme catalyzing the decarboxylation of pyruvate to acetate and CO₂ with quinone as an electron acceptor. Here, we investigate PQO activity in *Corynebacterium glutamicum*, examine purified PQO, and describe the crystal structure of the native enzyme and a truncated version. The specific PQO activity was highest in stationary phase cells grown in complex medium, lower in cells grown in complex medium containing glucose or acetate, and lowest in cells grown in minimal acetate-medium. A similar pattern with about 30-fold higher specific PQO activities was observed in *C. glutamicum* with plasmid-bound *pqo* expression under the control of the *tac* promoter, indicating that the differences in PQO activity are likely due to post-transcriptional control. Continuous cultivation of *C. glutamicum* at dilution rates between 0.05 and 0.4 h⁻¹ revealed a negative correlation between PQO activity and growth rate. Kinetic analysis of PQO enzymes purified from cells grown in complex or in minimal acetate-medium revealed substantial differences in specific activity (72.3 vs. 11.9 U·mg protein⁻¹) and turnover number (k_{cat} : 440 vs. 78 s⁻¹, respectively), suggesting post-translational modifications affecting PQO activity. Structural analysis of PQO revealed a homotetrameric arrangement very similar to the *Escherichia coli* pyruvate oxidase PoxB except for the C-terminal membrane binding domain, which exhibited a conformation markedly different from its PoxB counterpart. A truncated PQO variant lacking 17 C-terminal amino acids showed higher affinity to pyruvate and was independent of detergent activation, highlighting the importance of the C-terminus for enzyme activation and lipid binding.

Abbreviations

acetyl-CoA, acetyl-coenzyme A; ACK, acetate kinase; CGXII, minimal medium for *Corynebacterium glutamicum*; DCPIP, 2,6-dichloroindophenol; DDM, n-dodecyl-β-D-maltoside; DO, dissolved oxygen; DTT, dithiothreitol; E1p, E1 subunit of pyruvate dehydrogenase; FAD, flavin adenine dinucleotide; HRP, horseradish peroxidase; IMAC, immobilized metal ion affinity chromatography; IPTG, isopropyl-β-D-thiogalactopyranoside; MES, 2-(N-morpholino) ethanesulfonic acid; MPD, methylpentanediol; ODH, 2-oxoglutarate dehydrogenase; PDB, protein data bank; PDH, pyruvate dehydrogenase; PEG, polyethylene glycol; PEP, phosphoenolpyruvate; PoxB, pyruvate:quinone oxidoreductase from *Escherichia coli*; PP-binding domain, pyrophosphate-binding domain; PQO, pyruvate:quinone oxidoreductase from *Corynebacterium glutamicum*; PQO-Δ_{C17}, pyruvate:quinone oxidoreductase from *Corynebacterium glutamicum* lacking the last 17 amino acids at the C-terminus; PTA, phosphotransacetylase; Pyr-binding domain, pyrimidine-binding domain; Q8, ubiquinone 8; RMSD, root mean square deviation; rpm, rounds per minute; TCA, tricarboxylic acid; TEV, Tobacco etch virus; ThDP, thiamine pyrophosphate; TY, tryptone yeast; VE, volume exchange.

which oxidatively decarboxylates pyruvate to acetate with a naphthoquinone as an electron acceptor, and that is activated by detergents (e.g. Triton X-100), phosphatidylglycerol and dipalmitoyl-phosphatidylglycerol [26]. Like all known prokaryotic PQO enzymes, the active PQO of *C. glutamicum* is probably membrane-associated, it consists of four identical subunits (62 kDa each) and it utilizes thiamine pyrophosphate (ThDP), non-covalently bound flavin-adenine dinucleotide (FAD) and Mg^{2+} as cofactors [26,27]. The highest PQO activities were shown in extracts from cells grown in complex medium, about threefold lower activities were detected when the cells were cultured in minimal medium. Inactivation of the *pqo* gene resulted in the absence of the respective activity but did not affect the growth of *C. glutamicum*, showing that the enzyme is not essential under the tested conditions [28]. However, overexpression of the *pqo* gene in a PDHC-negative mutant of *C. glutamicum* resulted in 20-fold higher PQO activity and a partial restoration of the mutant's growth phenotype in complex medium [17], showing that high PQO activity together with the acetate-activating enzymes acetate kinase (ACK, EC2.7.2.1) and phosphotransacetylase (PTA, EC2.3.1.8) in complex medium may, at least partially, replace PDHC [28]. However, the physiological function of PQO in *C. glutamicum* remains unclear.

The most studied PQO to date is the orthologous PoxB from *Escherichia coli*, originally designated as pyruvate oxidase encoded by the corresponding *poxB* gene [29,30]. However, according to its activity as a quinone oxidoreductase [31–33] and in contrast to the actual pyruvate oxidases from lactic acid bacteria, that catalyze the formation of acetyl-phosphate, CO_2 and hydrogen peroxide in a phosphate and oxygen-dependent reaction [34–37], *E. coli* PoxB generates acetate while reducing quinones, and should therefore be considered as a PQO rather than a canonical pyruvate oxidase.

The biochemistry and catalytic mechanism of *E. coli* PoxB have been the subject of extensive research [e.g. 38–44; reviewed in 45], and its crystal structure was reported in 2008, both for the wild-type and a proteolyzed, activated form [46]. The first step of the PoxB reaction in the oxidative decarboxylation of pyruvate to acetate is the transfer of two electrons at the ThDP site to the adjacent, bound FAD cofactor. The reduction of flavin has been proposed to lead to a conformational change in the protein that exposes a C-terminal amphipathic helix with high lipid binding affinity; once PoxB attaches to the membrane, the electrons are transferred from FAD to ubiquinone 8 (Q8) in the electron transport chain. The *in vitro* activity of PoxB can be determined using a reductase assay in which soluble, synthetic electron acceptors (e.g.

ferricyanide) replace the physiological Q8. In the non-activated state the reductase activity of PoxB is low, but it increases dramatically by incorporation of lipids or detergents or by limited proteolysis with α -chymotrypsin (i.e., cleavage of the 23 C-terminal amino acids) in the presence of pyruvate and ThDP. However, despite all biochemical and structural studies, the physiological significance of PoxB in *E. coli* metabolism is not yet entirely clear.

As for the *E. coli* PoxB enzyme, the role of pyruvate oxidation by PQO in *C. glutamicum* metabolism has so far remained enigmatic. To get more insights into the structure and function of the PQO enzyme and its physiological role, we here took a comprehensive approach that includes a systematic analysis of its activity in wildtype and *pqo*-overexpressing *C. glutamicum* strains under different cultivation conditions and a systematic biochemical and structural analysis of purified wildtype PQO, as well as of a truncated version of the enzyme.

Results

Specific PQO activity in *C. glutamicum* is highest in complex medium and lowest in acetate minimal medium

In previous studies, no phenotype associated with the presence or absence of PQO was observed in *C. glutamicum* [26,28]. In this study, *C. glutamicum* wildtype, a PQO-deficient and PQO overproducer strains [*C. glutamicum* Δpqo and *C. glutamicum* Δpqo (pEKEx2-*pqo*), respectively] were cultivated either in 2xTY complex medium or in CGXII minimal medium with or without 1% acetate or 1% glucose, to decipher the possible effects of PQO deficiency and PQO overproduction compared to the wild-type strain. Under the conditions tested, no growth phenotype (growth rate and final optical density) was observed between the wildtype strain, *C. glutamicum* Δpqo and the PQO overproducer strain (data not shown).

Activity patterns in cell extracts of the three *C. glutamicum* strains were determined in both the mid-exponential and late stationary phases (24 h of cultivation) to gain insights into possible regulatory effects on PQO. Whereas the *pqo* deletion strain showed no detectable activity under all conditions tested, the wild-type strain showed the overall highest activity when cultivated in 2xTY medium at the stationary phase (~ 0.08 U·mg protein⁻¹) and the overall lowest activity when cultivated in acetate minimal medium both at the exponential and stationary phases (< 0.01 U·mg protein⁻¹) (Fig. 2). In contrast to the

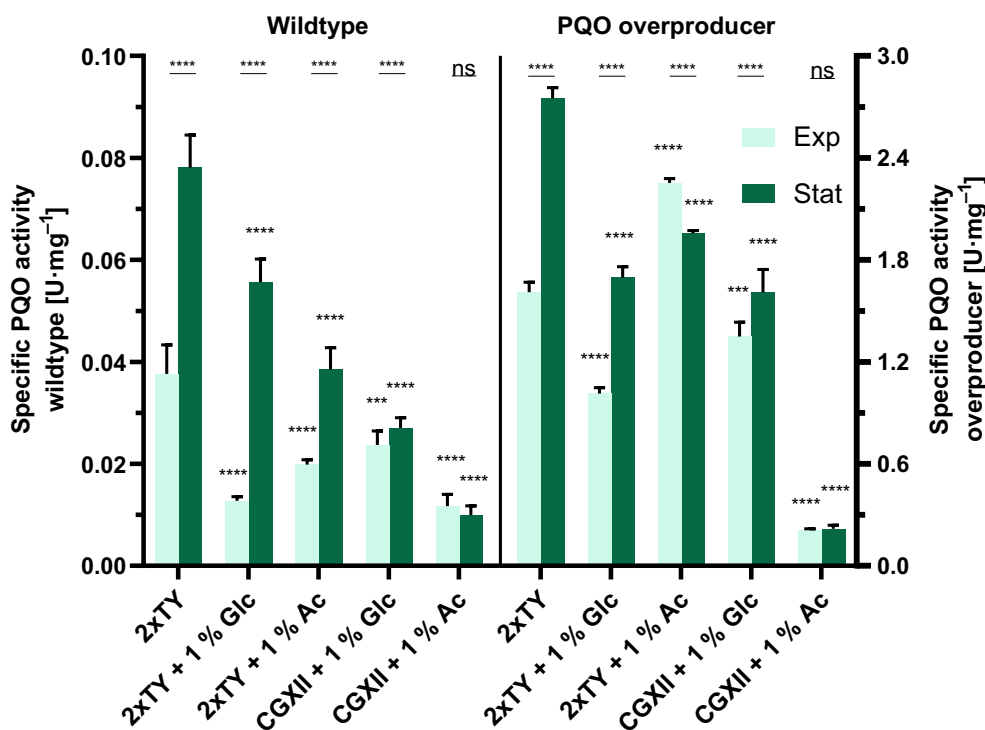


Fig. 2. Specific PQQ activity patterns. PQQ activities in cell extracts of *Corynebacterium glutamicum* (wildtype) and *C. glutamicum* Δpqo (pEKEx2-*pqo*) (PQQ overproducer) cultivated in different media and harvested at both the exponential (exp; light green) and stationary phase (stat, 24 h; dark green). The data are presented as the mean \pm SD ($N = 3$). Statistical analysis was conducted to compare PQQ activity across different growth medium conditions between exponentially grown and stationary cells. An ordinary two-way ANOVA followed by Bonferroni's post-test was used to calculate P -values adjusted for multiple comparisons, with the activity from cells grown in 2xTY medium serving as the control condition. Additionally, statistical analysis was performed to compare PQQ activity across different growth phases for cells cultivated under the same medium conditions. This was also analyzed using an ordinary two-way ANOVA followed by Bonferroni's post-test to calculate P -values adjusted for multiple comparisons ($***P < 0.0021$; $****P < 0.0001$; 'ns' indicates non-significant when $P > 0.05$, with underscored stars referring to statistical analysis for cells cultivated in the same medium but compared across growth phases). Ac, acetate; CGXII, minimal medium for *C. glutamicum*; Glc, glucose; TY, tryptone yeast extract.

specific PQQ activities in wildtype cells grown in minimal media, those observed in cells grown in 2xTY medium (independent of additional carbon source) were significantly higher (up to fourfold) in the stationary phase than in the exponential phase (Fig. 2). The addition of either 1% glucose or 1% acetate to 2xTY medium led to stepwise lower specific PQQ activities. When the wildtype was cultivated in acetate minimal medium, the activity was about twofold lower compared to the specific activity in cells cultivated in glucose minimal medium (~ 0.025 U·mg protein⁻¹ and ~ 0.01 U·mg protein⁻¹, respectively). Taken together, these results indicate that the corynebacterial PQQ activity is dependent on both the carbon source and the growth phase.

For the PQQ overproducer, the PQQ activity pattern was qualitatively similar to that of the wildtype, although the detected specific activities were up to 30-fold higher (Fig. 2). Although in cultivations with

2xTY medium \pm additional carbon source the effect of the growth phase was not as pronounced as for the wild-type, the highest difference in specific activity between cells from the exponential and from the stationary phase was still observed in 2xTY medium (~ 1.6 to 2.8 U·mg protein⁻¹, respectively). As for the wild-type strain, the overall highest PQQ activity was detected in 2xTY medium-cultivated cells in the stationary phase (~ 2.8 U·mg protein⁻¹) and the overall lowest at both growth phases in acetate minimal medium-grown cells (~ 0.2 U·mg protein⁻¹). Since in the PQQ overproducer strain of *C. glutamicum* the *pqo* gene expression is exclusively under control of the artificial P_{tac} promoter of the pEKEx2 plasmid, the different specific activities under the various conditions cannot be explained by transcriptional regulation but rather by posttranslational modification and thus, by different PQQ enzymes with respect to their biochemical properties.

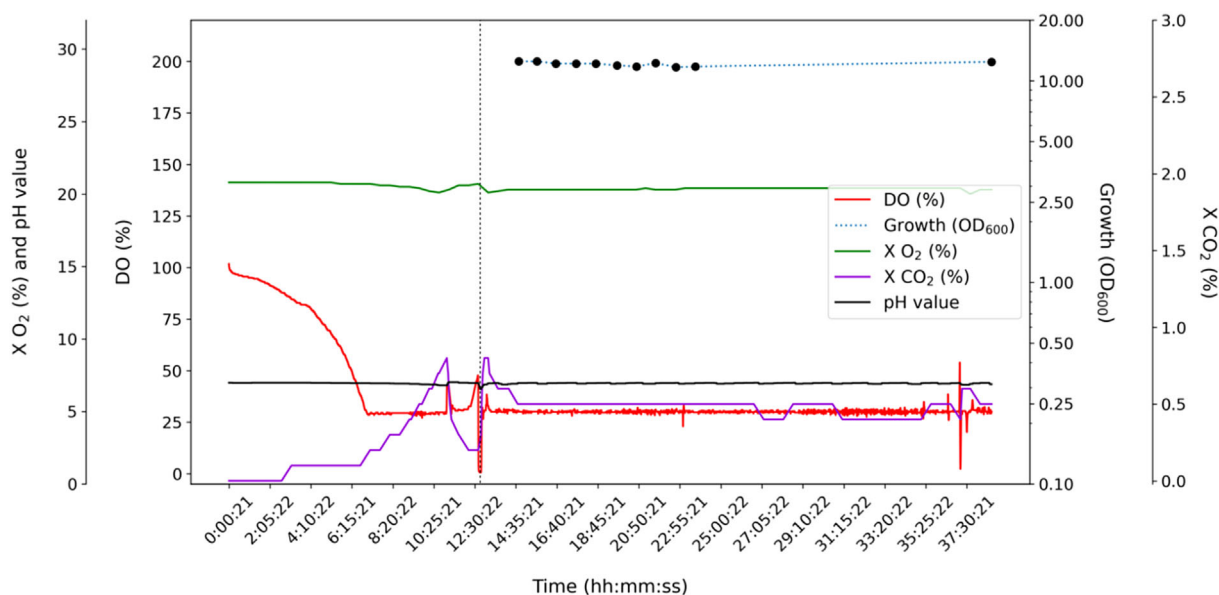


Fig. 3. Continuous cultivation of *Corynebacterium glutamicum*: growth and process parameters. Representative continuous cultivation of *C. glutamicum* in CGXII minimal medium supplemented with 1% glucose and 30 μg protocatechuic acid mL^{-1} at a dilution rate of 0.2 h^{-1} is shown ($N = 3$). The start of the continuous mode is marked by a dotted black vertical line. The graph plots the OD_{600} (black dots and blue dotted line) and the corresponding process data for dissolved oxygen (DO, red), pH value (black), and off-gas values for O_2 ($X \text{O}_2$, green) and CO_2 ($X \text{CO}_2$, purple) over time. In total, five volume exchanges were performed.

PQO cannot substitute for PDHC in *C. glutamicum*

It was previously shown that a *C. glutamicum* strain deficient of the E1p subunit of the PDHC (*C. glutamicum* $\Delta aceE$) was not able to grow on glucose as a sole carbon source and needed to be supplemented with acetate, in spite of the presence of PQO, ACK and PTA [28]. Here we tested whether plasmid-bound overexpression of *pqo* and thus, a surplus of PQO within the cells, restores the growth of *C. glutamicum* $\Delta aceE$ in minimal medium with glucose as the sole carbon source. For this purpose, we analyzed the growth of *C. glutamicum* wildtype and of *C. glutamicum* $\Delta aceE \Delta pqo$ (pEKEx2-*pqo*) in complex medium and in minimal glucose medium with/without supplementation of 150 mM acetate. *C. glutamicum* $\Delta aceE \Delta pqo$ (pEKEx2-*pqo*) showed restricted growth in complex medium and wildtype-like growth when acetate, or acetate plus glucose were added (data not shown). However, whereas *C. glutamicum* $\Delta aceE \Delta pqo$ (pEKEx2-*pqo*) grew well in minimal medium containing glucose and acetate, it did not grow at all in minimal medium containing glucose only (data not shown), suggesting that PQO may not be able to substitute for the PDHC.

The specific PQO activity of *C. glutamicum* is negatively correlated to the growth rate

Investigation of specific PQO activity in cell extracts of both wildtype and PQO overproducing strains of

C. glutamicum revealed that the specific activity in most media is generally higher during the stationary phase than during exponential growth (see above). This raised the question of whether the growth rate of the respective strain affects PQO activity. To examine the impact of growth rate on specific PQO activity in *C. glutamicum* wildtype systematically, we conducted continuous cultivation processes at different dilution rates ranging from 0.05 to 0.4 h^{-1} . For that purpose, the cultures were grown in CGXII minimal medium supplemented with 1% glucose using the DASGIP® Parallel Bioreactor System, as described in the [Materials and methods](#) section. The samples for the PQO activity determinations were taken at the beginning of the continuous cultivation (no volume exchange) and after the fifth total volume exchange for each dilution rate. An example of a continuous cultivation at a dilution rate of 0.2 h^{-1} is depicted in Fig. 3, with all monitored process parameters.

At the start of the different continuous growth cultivations, the specific PQO activities of *C. glutamicum* were comparable, ranging from 0.021 to 0.027 $\text{U} \cdot \text{mg protein}^{-1}$ (Fig. 4). At the end of each process (i.e., after 5 volume exchanges), the activities gradually decreased from 0.060 $\text{U} \cdot \text{mg protein}^{-1}$ at the lowest dilution/growth rate of 0.05 h^{-1} to a specific activity of 0.014 $\text{U} \cdot \text{mg protein}^{-1}$ at the highest dilution/growth rate of 0.4 h^{-1} . These findings suggest that the role of

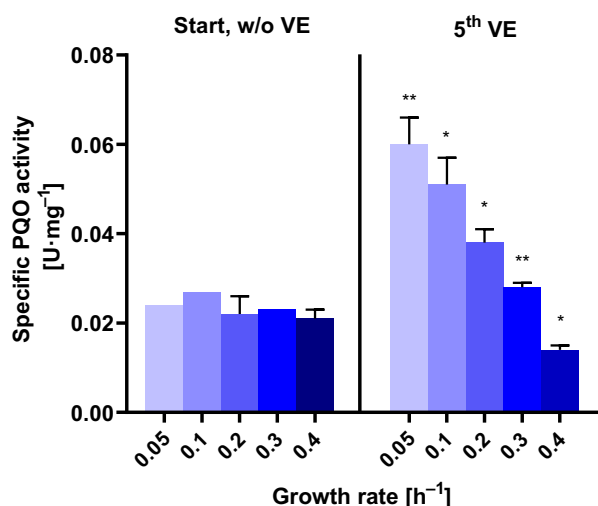


Fig. 4. Dependence of the growth rate on the specific PQQ activity of *Corynebacterium glutamicum* wildtype in continuous cultivation. The activity of PQQ in cell extracts from *C. glutamicum* was determined at the start [without volume exchange (VE)] and at the end of continuous cultivation (fifth VE), with dilution rates corresponding to the growth rates of the organism indicated below the bar charts. All cultivations were conducted in 1.5 L bioreactors within a DASGIP® Parallel Bioreactor System, at 30 °C, pH 7, and a constant dissolved oxygen level of 30% in CGXII minimal medium supplemented with 1% glucose and additionally 30 µg protocatechuic acid·mL⁻¹ in the feed solution during the continuous process. Error bars are shown for PQQ activity measurements performed in triplicate, and data presented as the mean ± SD ($N = 3$); otherwise, $N = 1$ (no error bars). To be noted, the ensemble of initial time points without VE (left) represents data points from equivalent batch cultures, on which a total of nine independent PQQ activity measurements (effective $N = 9$) were made with a mean of 0.023 ± 0.003 U·mg protein⁻¹. Statistical analysis was conducted to compare PQQ activity before and after initiating continuous feed at different dilution rates. An unpaired t -test followed by Bonferroni's post-test was used to calculate P -values adjusted for multiple comparisons ($*P < 0.05$; $**P < 0.0332$). Measurements at initial time points were minimized to reduce contamination risks during continuous cultivation.

the corynebacterial PQQ may be particularly relevant under conditions of low growth rates in *C. glutamicum*, shedding light on its potential physiological significance.

PQQ purified from cells grown in complex medium shows a sixfold higher turnover number compared to PQQ from acetate minimal medium-grown cells

To analyze the difference in specific PQQ activity in cells of the PQQ overproducer strain when cultivated in either 2xTY or in acetate minimal medium (Fig. 2),

the PQQ enzyme was purified natively from *C. glutamicum* $\Delta p q o$ (pEKEx2-*p q o*) cells, cultivated in the respective media, through the protocol established by Schreiner and Eikmanns [26]. The protocol exploits the specific PQQ binding to the detergent Triton X-114 in the presence of its substrate and cofactors; this property is reversible when substrate and cofactors are absent, allowing PQQ to be extracted back in the aqueous phase to homogeneity, as shown in the silver-stained gels after SDS/PAGE in Fig. 5. As shown in Table 1, the protein was enriched from both cell extracts 28- to 30-fold, showing different specific activities in all purification steps. In the Triton X-114 step, PQQ from 2xTY medium-grown cells displayed a specific activity of 72.3 U·mg protein⁻¹, whereas PQQ from acetate minimal medium-grown cells showed 11.9 U·mg protein⁻¹. K_m and k_{cat} values were determined for both PQQ variants with pyruvate as substrate (Table 2). Albeit sharing very similar K_m values (53 and 58 mM, respectively), the k_{cat} values differed significantly, showing an about sixfold difference in favor of PQQ from 2xTY medium-grown cells (440 s⁻¹ vs. 78 s⁻¹).

PQQ preparations from the *p q o*-overexpressing *C. glutamicum* cells grown in TY-medium and grown in acetate medium were also subjected to UV-absorbance analysis. Both spectra showed maxima at 380 and 450 nm, separated by a minimum at 415 nm (Fig. S1), as it is typical for flavin-containing enzymes and as shown before for TY-grown cells by Schreiner and Eikmanns [26]. The proportions were 0.76 mol FAD and 0.54 mol FAD per mol of PQQ subunit in the preparations from TY-grown and acetate-grown cells, respectively.

Structural analysis of PQQ

Crystals of PQQ were obtained in different conditions from protein purified by Triton X-114 extraction from *C. glutamicum* $\Delta p q o$ (pEKEx2-*p q o*) cells cultivated in 2xTY and harvested during the stationary phase. The crystal structure was first solved from a 2.5 Å resolution dataset collected from a crystal grown in the presence of 1 mM FAD, using the structure of *E. coli* PoxB as the search model. Isomorphous crystals were then obtained from protein purified by the same method, from cells grown in minimal acetate medium and diffracted up to 1.22 Å resolution (Table 3); the final model was therefore refined against this high-resolution dataset. Overall, the enzyme shows the same homotetrameric, 222 symmetrical arrangement observed for PoxB, with a single monomer in the asymmetric unit and the four protomers linked by

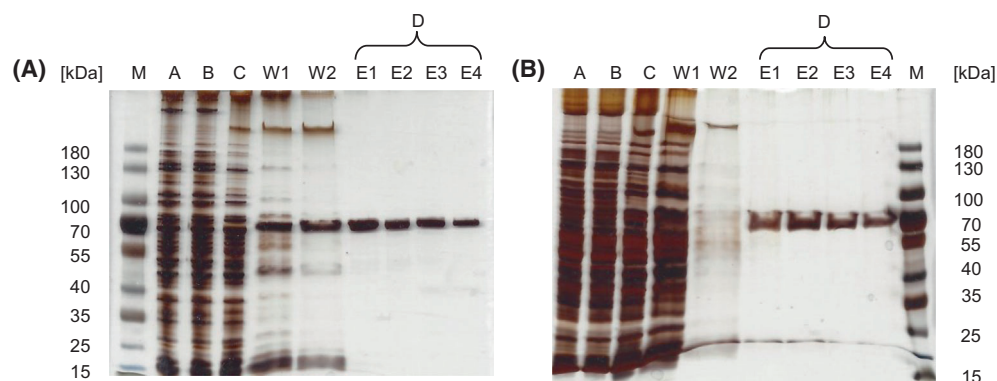


Fig. 5. Isolation of PQQ using Triton X-114 Extraction. Representative SDS/PAGE analysis of different purification steps of PQQ from *Corynebacterium glutamicum* Δpqo (pEKEx2-*pqo*) cells grown in 2xTY medium (A) or CGXII minimal medium with 1% acetate (B), harvested after 24 h. Lane M, Prestained Protein Ladder™; lane A, cell extract; lane B, supernatant after ultracentrifugation; lane C, supernatant after heat precipitation; lanes W1 and W2, waste fractions during triton X-114 extraction; lanes E1–E4, samples after Triton X-114 extraction, merged to one solution (D) ($N = 3$).

Table 1. Purification of PQQ from *C. glutamicum* Δpqo (pEKEx2-*pqo*), cultivated in either 2xTY medium (left values) or CGXII minimal medium with 1% acetate as carbon source (right values) and harvested in the stationary phase. The PQQ activities were determined in the presence of 0.5% DDM. The preparations after Triton X-114 extraction correspond to the purified PQQ enzymes.

Purification step	Total amount of protein (mg)	Total activity (U)	Specific activity (U·mg ⁻¹)	Recovery of activity (%)	Purification (fold)
Cell extract	393 503	1016 196	2.6 0.4	100 100	1 1
Ultra-centrifugation	262 470	850 190	3.2 0.4	84 97	1.3 1.1
Heat precipitation	128 209	678 171	5.3 0.8	67 87	2.0 2.0
Triton X-114 extraction	0.60 0.32	43.4 3.8	72.3 11.9	4.3 1.9	27.8 29.8

Table 2. Kinetic parameters of purified (full length) PQQ from *C. glutamicum* Δpqo (pEKEx2-*pqo*) cultivated in 2xTY medium and in CGXII minimal medium +1% acetate (Ac), and harvested after 24 h. Also shown are the kinetic parameters of purified PQQ- Δ_{C17} (a truncated version of PQQ) from *C. glutamicum* Δpqo (pEKEx2-*pqo*- Δ_{C17}). For the calculation of the k_{cat} values, a molecular weight of 247.8 kDa was assumed, corresponding to a tetramer of the enzyme.

PQQ variant	K_m (mM)	k_{cat} (s ⁻¹)	k_{cat}/K_m (s ⁻¹ ·M ⁻¹)
Full-length (2xTY)	53	440	8301
Full-length (CGXII + 1% Ac)	58	78	1344
Δ_{C17} (2xTY)	35	89	2514

crystallographic symmetry (Fig. 6A). The PQQ chain also shows the same domain organization as PoxB and the enzymes of this family, i.e. an N-terminal pyrimidine-binding domain (Pyr; residues 1–164), a central FAD-binding domain (FAD; residues 188–350) and a pyrophosphate binding domain (PP; residues 360–532), connected by flexible linkers (Fig. 6B). The

high-resolution electron density map pointed to the presence of a FAD molecule bound to the central domain, which could be traced unambiguously in an equivalent pose to *E. coli* PoxB (Figs S2 and S3). Noteworthy, the FAD isoalloxazinic group shows the typical ‘butterfly’ bent conformation of the three-ring system characterized by a $\sim 15^\circ$ deviation from planarity (Fig. S3), similar to previous observations on both *E. coli* PoxB and *Lactobacillus plantarum* pyruvate oxidase, in which the bent conformation was proposed to contribute to raise the FAD reduction potential [49]. It is noteworthy to mention that Sousa *et al.* [27] proposed a conserved motif, designated as “HEH lock” (in *E. coli* His49-Glu51-His80) and possibly involved in the dimerization process. A similar motif with a change of the first His to Asn can also be found in *C. glutamicum* PQQ (Asn48-Glu50-His79; Fig. S4).

In addition, and despite no ThDP had been added to the sample or the crystallization drops, analysis of the Fourier difference Fo-Fc map pointed to the presence of a low occupancy ThDP molecule, which could also be modeled in a conformation equivalent to the

Table 3. Crystallographic data collection and refinement statistics.

Dataset	PQO acetate med	PQO expr <i>E. Coli</i>	PQO_ <i>E. coli</i> _TPP	PQO- Δ_{C17} _TPP
Synchrotron beamline	ESRF ID23-1	ESRF ID30A-3	Soleil PX2A	ESRF ID30A-1
Wavelength (Å)	0.8856	0.9677	0.9763	0.9655
Space group	I 2 2 2	I 2 2 2	P 2 ₁	P 2 ₁
Unit cell parameters				
<i>a</i> , <i>b</i> , <i>c</i> (Å)	68.04, 119.07, 155.31	68.74, 120.02, 157.06	104.19, 77.94, 158.04	100.55, 98.48, 110.52
α , β , γ (°)	90.00, 90.00, 90.00	90.00, 90.00, 90.00	90.00, 100.63, 90.00	90.00, 90.84, 90.00
Resolution (Å) ^a	77.66–1.22 (1.32–1.22)	62.97–1.47 (1.67–1.47)	155.33–1.86 (2.06–1.86)	110.50–1.89 (2.02–1.89)
<i>R</i> _{pim} ^b	0.036 (0.616)	0.029 (0.325)	0.083 (0.538)	0.056 (0.498)
$\langle I/\sigma(I) \rangle$	10.8 (1.7)	12.9 (2.3)	5.8 (1.6)	7.3 (1.6)
Completeness (%)	94.1 (59.7)	94.7 (78.2)	94.7 (66.4)	95.4 (66.7)
CC(1/2)	0.997 (0.694)	0.997 (0.793)	0.990 (0.563)	0.995 (0.604)
Multiplicity	12.2 (12.6)	13.8 (11.3)	7.0 (7.4)	6.8 (7.2)
Refinement				
Resolution (Å)	17.67–1.22	21.33–1.47	155.33–1.86	37.46–1.89
No. reflections	144 896	66 252	134 984	133 646
<i>R</i> _{work} / <i>R</i> _{free} (%) ^c	17.6/19.2	16.3/19.0	20.7/24.0	16.8/19.7
No. atoms				
Protein	4323	4121	17 098	15 945
Ligands/ions	80	53	320	320
Solvent	592	621	1425	1005
Average B-factors				
Protein	18.3	27.3	32.8	38.3
Ligand/ions	14.9	16.9	22.2	29.7
Solvent	31.8	42.2	35.3	47.2
R.m.s deviations ^d				
Bond lengths (Å)	0.017	0.015	0.012	0.012
Bond angles (°)	1.77	1.51	1.50	1.52
Validation ^d				
MolProbity score	1.00	0.94	0.92	0.97
Clashscore	2.24	1.81	1.66	2.00
Poor rotamers (%)	0.42	0.46	0.89	1.02
Ramachandran plot ^d				
Favored (%)	98.96	98.72	98.30	98.64
Allowed (%)	0.87	1.28	1.53	1.13
Outliers (%)	0.17	0.00	0.17	0.23
PDB accession code	9EV3	9EV4	9EV5	9EV6

^aResolution limits were determined by applying an anisotropic high-resolution cut-off via STARANISO, part of the autoPROC data processing software [47]; values in parentheses refer to the highest resolution shell; ^b $R_{pim} = \sum_{hkl} [1/(N-1)]^{1/2} \sum_i |I_i(hkl) - \langle I \rangle(hkl)| / \sum_{hkl} \sum_i I_i(hkl)$, where *N* is the multiplicity, *I_i* is the intensity of reflection *i* and $\langle I \rangle(hkl)$ is the mean intensity of all symmetry-related reflections; ^c $R_{work} = \sum |F_o| - |F_c| / \sum |F_o|$, where *F_o* and *F_c* are the observed and calculated structure factor amplitudes. Five percent of the reflections were reserved for the calculation of *R_{free}*; ^dValues from MOLPROBITY [48].

one observed in *E. coli* PoxB (Fig. S2). A striking difference with respect to *E. coli* PoxB comes, however, from the conformation of the C-terminal, membrane interacting domain, which includes the α -peptide reported to be responsible for enzyme activation through interaction with the membrane [43]. In PQO, the C-terminal residues Ala564-Asn575 are well folded as an α -helix and are positioned on the opposite side of the long α -helix Arg328-Tyr349 with respect to full-length PoxB (Fig. 6C,D; Fig. S5). In the *E. coli* enzyme, in contrast, the residues Gly559-Thr568, supposed to fold as an amphipathic α -helix responsible

for membrane interaction, are part of an antiparallel β -sheet instead, that precedes the rather floppy C-terminal end (PDB: 3YE9). In corynebacterial PQO, the whole C-terminal domain, which could be traced entirely with the only exception of the C-terminal residue Pro579, adopts a radically different conformation with respect to the one observed in PoxB. Specifically, the 26-residue stretch that protrudes from the PP-binding domain (Asn533-Phe558) adopts an extended conformation that forms a long cap closing over the FAD-binding domain (Fig. 6C). In contrast to PoxB, however, no β -sheet structure could be observed, but a

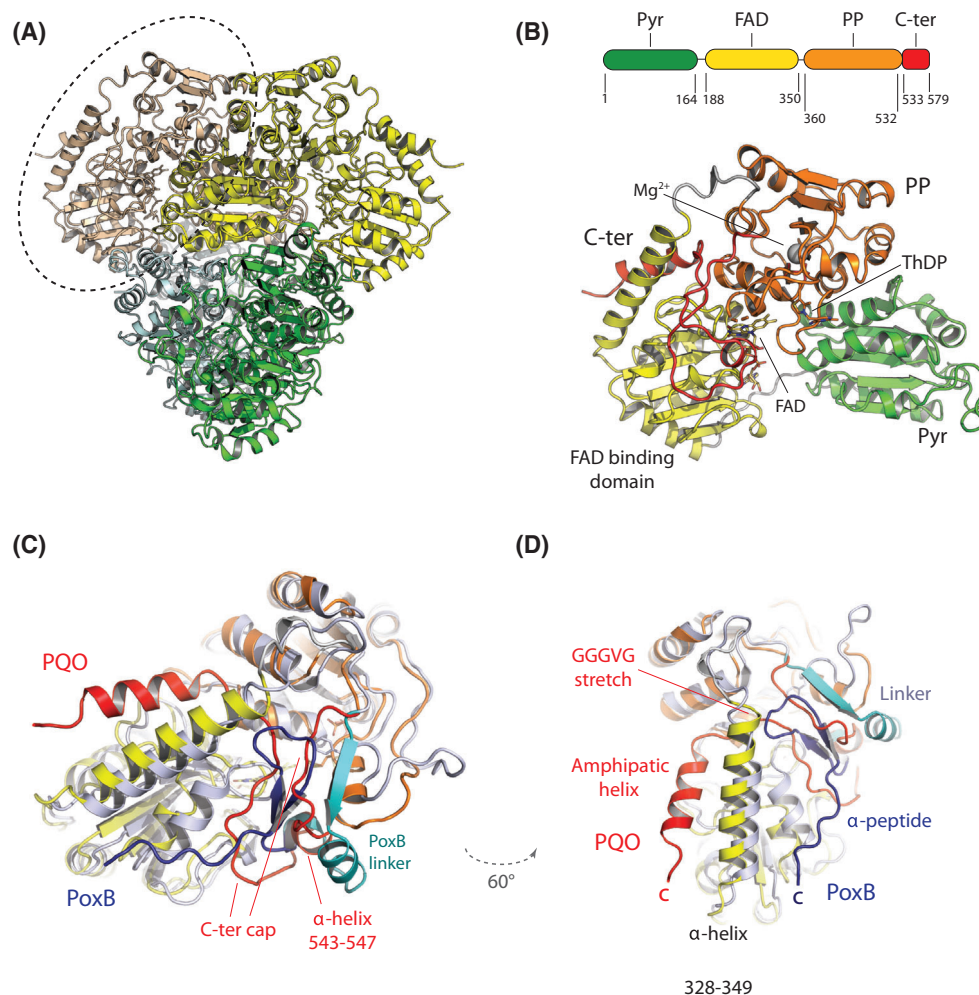


Fig. 6. Structural analysis of *Corynebacterium glutamicum* PQQ. (A) Cartoon overview of *C. glutamicum* PQQ homotetramer, colored per chain (light brown, yellow, green, cyan); the single protomers are related by crystallographic 222 symmetry. The dashed ellipse indicates the monomer shown in detail in (B). (B) Detailed view of a single PQQ monomer, same orientation as in (A). On the top, schematic representation of the domain composition along the polypeptide chain (FAD, FAD-binding domain; PP, pyrophosphate binding domain; Pyr, pyridine binding domain). The bound FAD and ThDP/Mg²⁺ cofactors are shown. (C, D) View of the C-terminal, membrane-interacting domain of PQQ [same domain coloring scheme as in (B)], upon superimposition to full-length *Escherichia coli* PoxB (gray; PDB: 3EY9). The C-terminal, membrane-anchoring domain of PoxB is shown in teal (linker region) and dark blue (α -peptide), respectively, while the whole C-terminal domain from PQQ is depicted in red. To note the very different conformation of this region and the unexpected position of the C-terminal, amphipathic helix in PQQ. structural figures were prepared with the software Pymol.

short α -helix between Trp543 and Met547 laying in a position close to PoxB Ser547-Leu551 (Fig. 6C). On the contrary, the Gly-rich stretch GGGVG, located between positions 559–563, crosses underneath the long Arg328-Tyr349 α -helix (Fig. 6D), making the C-terminal amphipathic α -helix to protrude from the opposite side. The helix extends till Asn575 and is followed by a short flexible tail to the C-terminal end (Fig. 6C,D).

To test whether such unexpected conformation of the C-terminal membrane-binding domain could be

the result of a conformational change triggered by the Triton X-114 extraction procedure, we overexpressed recombinant, N-terminal His₆-tagged *C. glutamicum* PQQ in *E. coli*. The enzyme was then purified by Ni²⁺ affinity chromatography, followed by TEV cleavage of the His₆ tag and size exclusion chromatography. The purified recombinant protein crystallized readily and generated not only crystals isomorphous to the ones obtained with the natively purified protein, but also a distinct crystalline form in the presence of supplied ThDP and Mg²⁺ (Table 3; Fig. S6). In either case, the

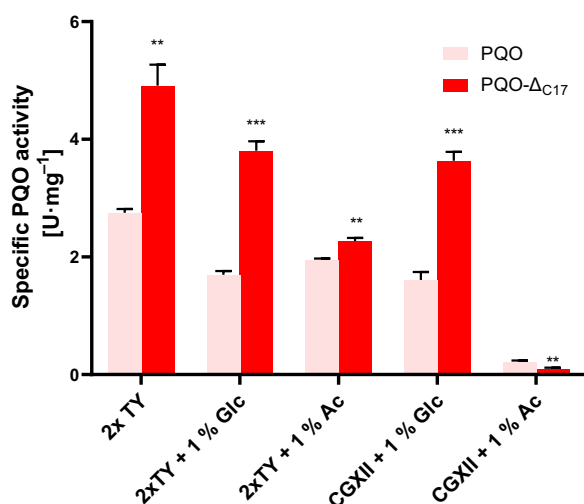


Fig. 7. Specific PQQ and PQQ-Δ_{C17} activity patterns. PQQ activity in cell extracts of *Corynebacterium glutamicum* Δ*pqo* (pEKEx2-*pqo*) (light red) or *C. glutamicum* Δ*pqo* (pEKEx2-*pqo*-Δ_{C17}) (red), cultivated in different media and harvested at the stationary phase. The data are presented as the mean ± SD (*N* = 3). Statistical analysis was conducted to compare PQQ activity across different growth medium conditions between stationary cells. An unpaired *t*-test followed by Bonferroni's post-test was used to calculate *P*-values adjusted for multiple comparisons (***P* < 0.0332; ****P* < 0.0021). Ac, acetate; CGXII, minimal medium for *C. glutamicum*; Glc, glucose; TY, tryptone yeast extract.

PQQ monomer is essentially identical to the high-resolution model determined from crystals of the native protein, to which it can be superimposed with an RMSD (over the ensemble of C α atoms) no higher than 0.4 Å. So does the whole C-terminal domain which adopts the same conformation described above, regardless of the presence of bound ThDP, indicating that such conformation is not induced by the detergent extraction procedure. The comparison between ThDP-bound *vs.* ThDP-deprived recombinant PQQ does not show significant conformational changes either, with the notable exception of residues Ser465-Glu486, corresponding to the active center loop in PoxB [46], which,

in the complex with ThDP-Mg²⁺, fold over the cofactor pyrophosphate-Mg²⁺ moiety (Fig. S6). In contrast, due to the lack of supporting electron density, the same residues could not be traced in the absence of bound ThDP, suggesting an intrinsic degree of flexibility in the absence of the ThDP cofactor. Consistently, in the high-resolution model of the natively purified protein where ThDP could only be modeled at incomplete occupancy, the same active center loop shows higher average B-factors (34.2 Å²) than the rest of the pyrophosphate-binding domain (17.1 Å²), consistently with its plasticity and suggesting that its closing is dependent on the presence of bound ThDP.

A C-terminal truncated PQQ is independent of detergent activation

The striking difference in the secondary structure and relative position of the C-terminal membrane binding domain, compared to *E. coli* PoxB, raised the question of the significance of this domain for the function and regulation of PQQ. To address this question, a truncated variant of *pqo* lacking the C-terminal 17 amino acids (corresponding to a cut at the Gly-rich stretch GGGVG) was constructed and overproduced in *C. glutamicum* Δ*pqo* (pEKEx2-*pqo*-Δ_{C17}). The PQQ-Δ_{C17} overproducer was cultivated under different conditions and PQQ activities were determined in the stationary phase (24 h of cultivation) and compared to those of the strain carrying the plasmid-encoded, wild-type *pqo* gene. No growth phenotype of *C. glutamicum* Δ*pqo* (pEKEx2-*pqo*-Δ_{C17}) was observed under the conditions tested, except in extracts of cells grown in the presence of acetate, where the PQQ activities detected in extracts of stationary phase cells were more than two-fold higher for the PQQ-Δ_{C17} variant (Fig. 7). For further analysis, PQQ-Δ_{C17} was purified from the overproducer strain cultivated in 2xTY medium to the late stationary phase. As shown in Table 4, the truncation of the last 17 amino acids in PQQ-Δ_{C17} led to a significantly lower recovery of protein through the

Table 4. Purification of PQQ-Δ_{C17} from *C. glutamicum* Δ*pqo* (pEKEx2-*pqo*-Δ_{C17}), cultivated in 2xTY medium and harvested in the stationary phase. In brackets are values for the purification of full-length PQQ from *C. glutamicum* Δ*pqo* (pEKEx2-*pqo*) under the same conditions, see also Table 1. The PQQ activities were determined in the presence of 0.5% DDM.

Purification step	Total amount of protein (mg)	Total activity (U)	Specific activity (U·mg ⁻¹)	Recovery of activity (%)	Purification (fold)
Harvesting of cell extract	304 (393)	1480 (1016)	4.3 (2.6)	100 (100)	1 (1)
Ultra-centrifugation	288 (262)	1191 (850)	4.1 (3.2)	80 (84)	0.95 (1.3)
Heat precipitation	76 (128)	780 (678)	10.3 (5.3)	53 (67)	2.4 (2.0)
Triton X-114 extraction	0.12 (0.60)	2.4 (43.4)	20.0 (72.3)	0.16 (4.3)	4.6 (27.8)

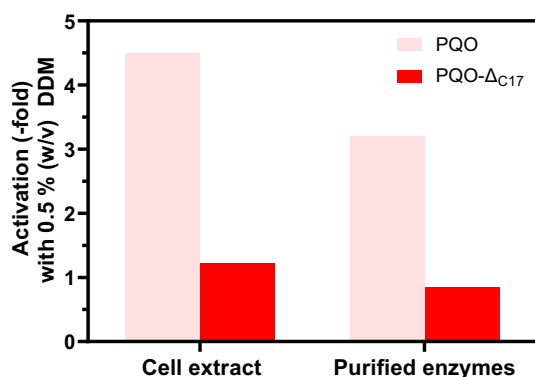


Fig. 8. Activation of *Corynebacterium glutamicum* PQQ by *n*-Dodecyl- β -D-maltoside (DDM). Enzyme activity was determined in cell extracts of 2xTY medium-grown cells (24 h) of *C. glutamicum* Δpqo (pEKEx2-*pqo*) (light red) and *C. glutamicum* Δpqo (pEKEx2-*pqo*- ΔC_{17}) (red) in the DCPIP reductase assay with and without the detergent DDM. Also shown is the activation of purified PQQ and PQQ- ΔC_{17} . The specific activities of PQQ and PQQ- ΔC_{17} in cell extracts, in the absence of DDM, were 0.58 and 3.52 U-mg protein⁻¹, respectively ($N = 2$). For the purified enzymes, their specific activities, in the absence of DDM, were 22.6 and 23.4 U-mg protein⁻¹, respectively ($N = 2$).

Triton X-114 extraction procedure, which yield ranged from about 0.15% (0.60 mg out of 393 mg protein) for full-length PQQ to about 0.04% for PQQ- ΔC_{17} (0.12 mg out of 304 mg total protein). This finding suggests that the truncated variant was significantly impaired in its interaction with the detergent Triton X-114. In cell extracts, the truncated PQQ displayed higher specific activity (4.3 U-mg protein⁻¹) compared to the full-length PQQ (2.6 U-mg⁻¹), and was not dependent on the presence of DDM, unlike full-length PQQ, which was activated about 4.5-fold (Fig. 8). However, when comparing purified enzymes, full-length PQQ exhibited a specific activity of 72.3 U-mg protein⁻¹ vs. 20.0 U-mg protein⁻¹ for the C-terminal truncated variant. The kinetic properties of PQQ- ΔC_{17} were determined and revealed an approximately five-fold lower k_{cat} (89 s⁻¹ vs. 440 s⁻¹) and an about 1.5-fold lower K_m value (35 mM vs. 53 mM) compared to full-length PQQ from 2xTY medium-grown cells (Table 2). Taken together, these results strongly suggest that the C-terminal 17 amino acids within the PQQ enzyme are crucial for detergent/lipid binding and that interaction with lipids is involved in the activation of the enzyme.

To explain these observations and get more insights into the PQQ conformational landscape, PQQ- ΔC_{17} was also structurally characterized. The mutant protein was purified as an N-terminal His₆-tagged protein from an overexpressing *C. glutamicum* strain,

followed by TEV cleavage of the tag (Fig. 9). Diffracting crystals were only obtained when purified PQQ- ΔC_{17} was supplied with 2 mM ThDP and 5 mM MgCl₂ (Table 3), suggesting a decreased enzyme stability in the absence of the thiamine cofactor. The structure, solved at 1.9 Å resolution, showed the canonical PQQ tetramer in complex with FAD and ThDP-Mg²⁺ (Fig. S7), while the polypeptide chain could be traced until the C-terminal end of the PP-binding domain (no further than residue Pro538 for subunit D). No supporting electron density was detected for the C-terminal domain (Fig. S7), suggesting that the cap that precedes the amphipathic helix (Fig. 6C) becomes too mobile in the absence of the Gly-rich stretch that anchors it under the α -helix Arg328-Tyr349. Otherwise, no significant conformational change could be detected with respect to the wild-type enzyme, with the single PQQ- ΔC_{17} monomers that could be superimposed to the high-resolution full-length structure with RMSD between 0.43 and 0.66 Å. Noteworthy, no conformational difference could be observed for the active center loop, in contrast to proteolytically activated PoxB which showed a structural rearrangement of Phe465 that makes it occupy a favorable position for electron transfer from the thiamine to the FAD cofactor [46]. In *C. glutamicum* PQQ, such residue is replaced by Met468 which occupies a structurally equivalent position to Phe465 in the activated form of PoxB (PDB: 3EY9), and this in all PQQ structures, including PQQ- ΔC_{17} , in which the active center loop was traceable (Fig. S8). These observations suggest that either Met468 may not be involved in electron transfer between cofactors in PQQ, or that corynebacterial PQQ, unlike PoxB, might have crystallized into an active state regardless of the expression host and purification procedure. In this case, the observed membrane-binding domain conformation, and more specifically the C-terminal amphipathic helix, may be indicative of a membrane-interacting state of the enzyme.

Discussion

The study presented here aimed to get more insights into the role of PQQ in *C. glutamicum* by following and comparing specific PQQ activities in the wild-type, in a PQQ-deficient and in a *pqo*-overproducing strain, grown under different conditions. The biochemical and structural features of purified native PQQ and the truncated variant PQQ- ΔC_{17} were also determined, showing unexpected features which differ from those of the model PQQ enzyme PoxB from *E. coli* and raise new questions on the activation mechanism.

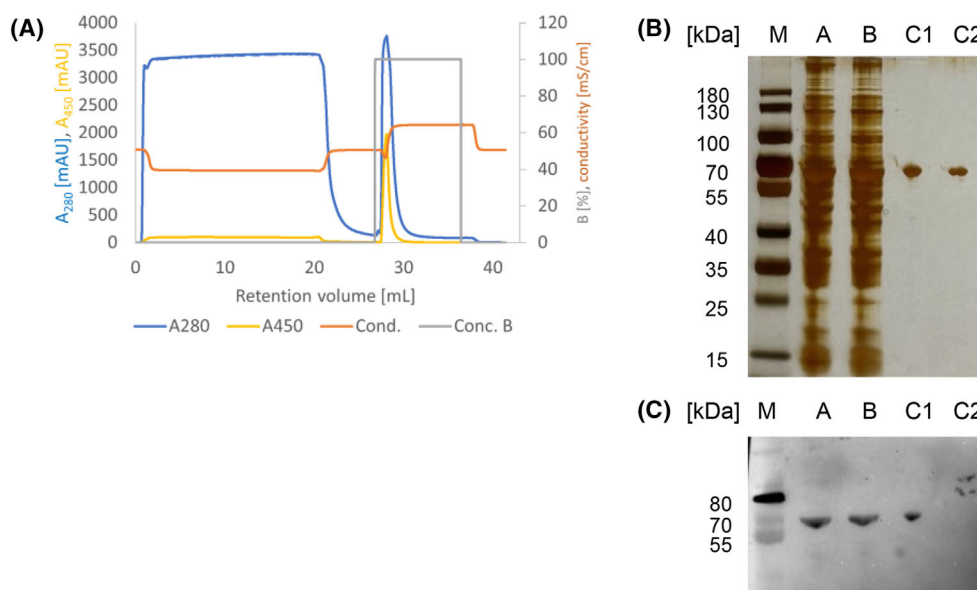


Fig. 9. Purification of an N-terminally His₆-tagged PQQ- Δ C₁₇ variant from *Corynebacterium glutamicum* using Ni²⁺-NTA chromatography. (A) Purification of His₆-tagged PQQ- Δ C₁₇ from crude extracts of *C. glutamicum* Δ pqo (pEKEx2-*his*₆-TEV-*pqo*- Δ C₁₇) cells grown in 2xTY medium, harvested after 24 h. Shown is absorbance at 280 nm (blue, left y-axis) and 450 nm (yellow, left y-axis). Percentage of applied elution buffer (gray, right y-axis) and conductivity (orange, right y-axis) are also shown. (B) SDS/PAGE-analysis and (C) Western blot against His₆-tag of different purification steps of His₆-tagged PQQ- Δ C₁₇. Lane A, cell extract; lane B, supernatant after ultracentrifugation; lane C1, sample after Nickel-NTA chromatography; lane M*, iBright™ Prestained Protein Ladder; lane M, Prestained Protein Ladder™; lanes C2, sample after TEV-protease treatment and subsequent separation through a 100 kDa cut-off filter.

While glycolysis and oxidative decarboxylation of pyruvate by the PDHC are common and well-studied in many bacteria [reviewed in 14], little is known about the nature and the role of the alternative pyruvate oxidation pathway catalyzed by PQQ. Sousa *et al.* [27] recently reviewed the amino acid conservation and taxonomic distribution of PQQs, describing these enzymes as exclusively present in prokaryotes and showing that they have highly conserved regions around the ThDP and FAD binding sites, but not at the C-terminus. As also mentioned by the authors, *E. coli* PoxB has been the best-studied PQQ enzyme to date, where it functions to transfer two reducing equivalents from the cytosol to the respiratory chain via quinols, supposedly as a backup system for the PDHC reaction [27]. The physiological significance of this process in *E. coli* is, however, not yet entirely clear. Abdel-Hamid *et al.* [50] showed that PoxB in combination with acetyl-CoA synthetase can replace the PDHC, is advantageous for aerobic growth in glucose minimal medium and is important for survival of the cells when other pyruvate-decarboxylating enzymes (PDHC or pyruvate formate lyase) are not functional. Moreover, Li *et al.* [51] reported that a *poxB* mutant shows reduced glucose uptake, reduced activity of TCA cycle enzymes, lower growth rates, lower growth yields and lower

carbon turnover rates than the wild type and Moreau proposed a protective role of PoxB against oxidative stress by decreasing the formation of NADH in non-growing *E. coli* cells [52]. All these observations indicate a significant participation of PoxB in carbon metabolism and/or during oxidative stress.

In *C. glutamicum*, PQQ in combination with ACK and PTA also theoretically offers a bypass or a support for the PDHC reaction, providing acetyl-CoA and reducing equivalents to the respiratory chain. However, a *pqo*-deficient mutant displayed no significant phenotype under all conditions tested here, as well as in our previous study [28], and overexpression of *pqo* only slightly complemented the growth deficit shown by a PDHC-deficient strain in complex medium, suggesting a minor involvement of PQQ to compensate for PDHC deficiency [28]. Consistently, we show here that the PDHC-deficient strain could not grow solely in glucose minimal medium, and that even *pqo* overexpression is not enough to alleviate the need for acetate supplementation. These observations indicate that, under the tested conditions, PQQ activity is irrelevant. Thus, available evidence indicates PDHC as the primary and essential enzyme in *C. glutamicum* for generating acetyl-CoA during growth on carbohydrates that do not enter the central carbon metabolism

pathways other than by direct conversion to acetyl-CoA (such as acetate or ethanol). Given that the typical intracellular pyruvate level in growing *C. glutamicum* cells ranges from 0.05 to 0.8 mM [53,54] and considering the relatively high affinity of the PDHC for pyruvate ($K_m = 1.7$ mM) [17], the low substrate affinity of PQQ for pyruvate ($K_m = > 50$ mM) is also consistent with this enzyme playing a minor role in pyruvate decarboxylation under canonical growth conditions. This finding aligns with the notion that conversion of pyruvate to acetyl-CoA via PQQ, ACK, and PTA is energetically less efficient than via PDHC, given the ATP requirement for acetate activation. However, the deletion of the *pqo* gene in PDHC-deficient production strains of *C. glutamicum* had a positive effect on the production of L-lysine, 2-ketoisovalerate and isobutanol [55–57]. This effect could be explained by the fact that during the stationary phase (i.e. the production phase), the intracellular pyruvate concentration in the parental PDHC-deficient strain is much higher than during the growth phase (26 mM vs. 0.05 mM) [54], suggesting that, under those conditions, PQQ may be competing for pyruvate to the detriment of other synthetic pathways.

In spite of the apparent dispensability of PQQ, our data on PQQ activities in *C. glutamicum* wildtype indicate (i) that the enzyme is present under all conditions tested and (ii) that the specific *in vitro* activity in cell extracts varies significantly with the growth media, the growth phases and the growth rates in glucose-limited continuous cultivations. The overall lowest PQQ activity levels were observed in cells grown in acetate minimal medium and at the highest growth rate (0.4 h⁻¹) in glucose minimal medium. The different specific PQQ activities in *C. glutamicum* may indicate a regulatory connection between PQQ activity and metabolic flux within the TCA cycle and/or that towards pyruvate. At the level of citrate synthase, the specific *in vivo* activity of the TCA cycle was found to be about fourfold higher in cells grown in minimal medium containing acetate (413 mU·mg protein⁻¹) than in cells grown in minimal medium containing glucose (111 mU·mg protein⁻¹) and, *vice versa*, the total *in vivo* pyruvate formation rate was threefold lower in cells growing on acetate than in cells growing with glucose (72 mU·mg protein⁻¹ vs. 227 mU·mg protein⁻¹, respectively) [8]. In accordance, the specific activities of several TCA cycle enzymes (aconitase, EC4.2.1.3; succinate dehydrogenase, EC1.3.5.1; malate:quinone oxidoreductase, EC1.1.5.4; malate dehydrogenase, EC1.1.1.37) in cell extracts and the expression of the respective genes were found to be higher when *C. glutamicum* cells grow in acetate minimal medium [58,59; reviewed in

15,60]. Moreover, Graf *et al.* [61] found an inverse relation between *pqo* transcript levels and the growth rate in glucose-limited chemostat cultivations, reporting an increase of the concentrations of most of the TCA cycle intermediates with increasing growth rates of *C. glutamicum*. Taken together, the available data suggest a possible negative correlation between PQQ and TCA cycle activity and, conversely, a positive correlation between PQQ activity and pyruvate availability.

The PQQ activity data with the wildtype and the *pqo*-overexpressing strain of *C. glutamicum* and in particular the biochemical analysis of purified PQQ enzymes from cells grown in complex and in minimal acetate medium suggest that PQQ activity may be regulated by post-translational modifications or by allosteric control. Although our kinetic analyses on PQQ variants revealed similar K_m values, yet the k_{cat} values varied markedly, with PQQ from complex medium-grown cells displaying approximately sixfold higher specific activity compared to that from acetate minimal medium-grown cells. Phosphorylation, acetylation, succinylation and also pupylation and mycoloylation of proteins have been documented in *C. glutamicum* [62–68]. In this respect, the study by Mizuno *et al.* [63] which described the changes in the acylome of *C. glutamicum* under glutamate production conditions and identified several hundred acetylated and/or succinylated proteins, identified PQQ as acetylated at lysine residues K19 and K304, and only under glutamate-producing conditions, also succinylated K213. However, the study did not provide quantification of these modifications on PQQ, which significance remains unclear. In spite of the high resolution achieved, we were not able to model unambiguously any post-translational modification on PQQ models obtained from enzyme samples purified and crystallized from acetate- or complex medium-grown *C. glutamicum* cells, possibly due to lack of homogeneity in post-translational modifications in the studied samples. Thus, the nature and role of such modifications in PQQ remain to be elucidated.

The *C. glutamicum* PQQ structure was solved at a resolution of down to 1.22 Å, based on diffraction sets obtained from PQQ purified from cells grown in acetate minimal medium. Although corynebacterial PQQ is very similar to *E. coli* PoxB in terms of overall fold and quaternary structure, subdomain composition and cofactors requirement, the C-terminal membrane-binding domains of PQQ and PoxB were found to differ significantly, despite a supposedly similar activation mechanism triggered by FAD reduction and protein-membrane interactions. The orientation of the

amphipathic C-terminal α -helix in PQQ, responsible for membrane interactions and well-folded in all the crystal structures reported here, also contrasts with the direction of the corresponding residues in PoxB. Prompted by such differences, we analyzed whether AlphaFold2 [69] may be able to predict a different conformational state for PQQ, specifically with respect to its C-terminal membrane-binding domain. The AlphaFold2 PQQ monomeric model, accessible online at the EBI AlphaFold Protein Structure database (Uniprot accession no. Q8NMG5; Fig. S9), exhibits high pLDDT values (> 90) for most of the protein chain, and overall agrees very well with the highest resolution experimental structure (PQQ purified from acetate minimal medium, in complex with FAD and ThDP-Mg²⁺), to which it can be superimposed with an RMSD value of around 0.7 Å (Fig. S9). Nonetheless, two specific areas in the AlphaFold2 model are characterized by low pLDDT values (< 70), one spanning residues Ser343-His356, the other the whole C-terminal membrane binding region, i.e. residues Leu535 to the C-terminal Pro579. Failure by AlphaFold2 to predict a reliable secondary structure of the PQQ C-terminal domain is suggestive of a certain degree of plasticity of this domain, consistently with its role in reversible protein-membrane interactions and with the PoxB activation model. How this domain contributes to PQQ interactions with the bacterial cell membrane in *C. glutamicum* remains to be established.

The distinct C-terminal structure of PQQ from *C. glutamicum*, particularly the unique positioning of its terminal amphipathic α -helix, raises questions about its functional implications. To confirm whether this conformation may have been a result of the Triton X-114 extraction process, we purified a His₆-tagged PQQ variant from an *E. coli* strain, cleaved off the tag and analyzed it by X-ray crystallography. The structure was indistinguishable from the native PQQ, confirming that the unique conformation of its C-terminal membrane anchoring domain is an inherent characteristic, regardless of the purification procedure. The drastic difference at the C-terminus between PQQ and PoxB is unexpected, given that sequence and overall structural homology, together with enzymatic data, would predict a conserved activation mechanism. To further decipher the functional importance of the α -helix at the C-terminus of *C. glutamicum* PQQ, we constructed and analyzed a truncated variant (PQQ- Δ_{C17}) lacking the carboxy-terminal 17 amino acids, and confirmed that these residues are crucial for lipid/detergent interaction and enzyme activation. Three key observations support this conclusion: (a) purification of PQQ- Δ_{C17} using Triton X-114 resulted in substantially lower recovery than

that of the full-length PQQ, (b) the specific activity of PQQ- Δ_{C17} in cell extracts was in general higher than that of the full-length PQQ and (c) its activity was independent of DDM activation. Despite the structure of PQQ- Δ_{C17} did not show major differences with respect to the full-length enzyme, it is noteworthy to mention that diffracting crystals were only obtained in the presence of 2 mM ThDP and 5 mM MgCl₂, which could indicate a somehow decreased enzyme stability in the absence of the thiamine cofactor.

Taken together, our findings offer vital insights into the structure and function of the PQQ from *C. glutamicum*, however, while biochemically and structurally well characterized in this and previous work, the physiological role of PQQ in *C. glutamicum* is yet to be determined.

Materials and methods

Strains, cultivation conditions, plasmids and oligonucleotides

Bacterial strains and plasmids employed in this study are listed in Table S1. For cultivation of all *C. glutamicum* strains, either 2xTY complex medium or CGXII minimal medium [70] with 1% glucose and/or 1% acetate as carbon source(s) were used. *C. glutamicum* was cultivated aerobically at 30 °C in 50 mL cultures in 500 mL baffled Erlenmeyer flasks. *E. coli* DH5 α strains were cultivated aerobically in 5 mL 2xTY medium at 37 °C in test tubes. When needed, kanamycin was added at a concentration of 50 $\mu\text{g}\cdot\text{mL}^{-1}$. For strains carrying the pEKEx2 plasmid, overexpression of genes was induced by adding 0.5 mM isopropyl- β -D-thiogalactopyranoside (IPTG) to the culture.

Oligonucleotides used in this work are listed in Table S2 and were designed using the NEBuilder tool from New England Biolabs. For the construction of pET28a (+)-TEV--*pqo*- Δ_{C17} , oligonucleotides pET28a-TEV_lin_fwd and pET28a-TEV_lin_rev were used to obtain linearized pET28a-TEV as a vector backbone via PCR. *Pqo*- Δ_{C17} _in28a_fwd and *pqo*_in28a_rev were used in a PCR to amplify the gene coding for the PQQ lacking the last 17 amino acids from *C. glutamicum* DNA. Both fragments were ligated by Gibson assembly and chemo-competent *E. coli* DH5 α cells were transformed with this ligation reaction. Plasmid isolation from *E. coli* was performed according to instructions of the “NucleoSpin Plasmid, Mini kit for plasmid DNA” (Macherey-Nagel, Düren, Germany). For creating pEKEx2-*his*₆-TEV-*pqo*- Δ_{C17} , plasmid pET28a (+)-TEV-*pqo*- Δ_{C17} was used as a template in a PCR with oligonucleotides px2_His-TEV-*pqo* Δ_{C17} _fwd and px2_His-TEV-*pqo* Δ_{C17} _rev for the amplification of a sequence containing a N-terminal His₆-tag and TEV-cleavage site plus the sequence for PQQ- Δ_{C17} . This fragment was ligated into a *Sac*I-linearized pEKEx2 vector by Gibson

assembly as described before. For generation of pEKEx2-*pqo*- Δ_{C17} , oligonucleotides delta_C1_fwd and delta_C1_rev, as well as delta_C2_fwd delta_C2_rev were used in a PCR to amplify the pEKEx2-*pqo* vector in two fragments which ultimately lack only the sequence coding for the last 17 amino acids in PQO. These fragments were ligated by Gibson assembly as described before. Electro-competent *C. glutamicum* cells were transformed with DNA using a standard protocol [71].

Continuous cultivation

In order to generate sufficient biomass, a batch process was performed using a pre-culture of *C. glutamicum* wildtype to inoculate 700 mL of CGXII medium with 1% glucose to an OD₆₀₀ of 0.3. The culture was maintained in a 1.5 L bioreactor within a DASGIP® Parallel Bioreactor System (Eppendorf, Hamburg, Germany), at 30 °C, pH 7, and a constant dissolved oxygen (DO) level of 30%. Struktol® J 647 (Schill/Seilacher, Hamburg, Germany) was added to prevent foam over. After the culture reached the early stationary phase, continuous cultivation was started by adjusting the dilution rate to 0.05, 0.1, 0.2, 0.3 h or 0.4 h⁻¹, respectively, using an external pump to continuously feed CGXII medium with 1% glucose and 30 µg protocatechuic acid·mL⁻¹ from a 10 L bottle, and another external pump for harvesting to maintain a constant reaction volume in the bioreactor. The continuous cultivations were performed at a constant pH of 7, a constant DO level of 30%, and a stirrer cascade (150–900 rpm) at 30 °C. Sterile controls were conducted after each total volume exchange to confirm the process was free of contaminants. The continuous cultivation was stopped after the fifth volume exchange.

Enzyme assays

To obtain cell extracts for PQO activity determinations, cells were disrupted as described previously [26]. The cell extracts were analyzed for PQO activity by using the following test buffer in pre-heated cuvettes at 30 °C: 100 mM MES [2-(N-morpholino) ethanesulfonic acid; pH 6.0], 10 mM MgCl₂, 0.1 mM thiamine pyrophosphate (ThDP), 0.5% (wt/vol) n-Dodecyl-β-D-maltoside (DDM), 0.3 mM 2,6-dichloroindophenol (DCPIP), 100 mM sodium pyruvate, and appropriate amounts of cell extract. After pyruvate addition, the reduction of DCPIP was monitored photometrically at 600 nm at 30 °C. PQO activity is represented in units per milligram of protein, where 1 U is defined as 1 µmol of DCPIP reduced per min ($\epsilon_{600} = 22 \text{ mM}^{-1} \cdot \text{cm}^{-1}$).

Purification of PQO and His₆-PQO- Δ_{C17}

To purify PQO natively from *C. glutamicum* strains, extracts of cells (obtained as described above) were

ultracentrifuged (180 000 g, 1.5 h) and the supernatant was collected. A heat precipitation step (49 °C, 3 min) was performed, and the sample was ultracentrifuged (100 000 g, 50 min). With the resulting supernatant, the Triton X-114 extraction method was applied as described before [26,72]. Purified samples were kept in 100 mM MES (pH 6.0) with 10% glycerol.

The UV-visible spectra of PQO preparations were taken with a NanoDrop 2000 (Thermo Scientific, Waltham, MA, USA). After heat denaturation of the enzyme preparations by incubation for 10 min at 95 °C, the content of the released FAD per PQO monomer was quantified photometrically (using the maxima at 450 nm and the protein content of the preparations).

For purification of His₆-tagged PQO- Δ_{C17} from *C. glutamicum* Δ_{pqo} (pEKEx2-*his₆*-TEV-*pqo*- Δ_{C17}), cells were disrupted as described above, except that the cells were resuspended in binding buffer [20 mM sodium phosphate buffer (pH 7.4), 500 mM sodium chloride, 40 mM imidazole]. Cell extracts were ultracentrifuged, and heat precipitation was performed as described above. Next, nickel-affinity chromatography was conducted by applying the sample through a 50 mL super-loop to a 1 mL HisTrap FF column (Cytiva, Uppsala, Sweden), pre-equilibrated with binding buffer, on an ÄKTA pure system. His₆-tagged PQO- Δ_{C17} was eluted by applying 100% of elution buffer [20 mM sodium phosphate buffer (pH 7.4), 500 mM sodium chloride, 400 mM imidazole]. To remove imidazole, a 30 kDa cut-off filter (Amicon Ultra-15, Merck, Darmstadt, Germany) was used and the retained sample was resuspended in 25 mM sodium phosphate buffer (pH 7.4), 125 mM sodium chloride, and 5 mM DTT. The His₆-Tag was consequently removed with TEV-protease and a 100 kDa cut-off filter (Vivaspin 2, Sartorius, Göttingen, Germany) was used to separate PQO- Δ_{C17} from the His₆-tag and the TEV-protease. The retained sample was resuspended in 100 mM MES (pH 6.0) with 10% glycerol. The removal of the His₆-tag was confirmed using Western blot analysis as previously described [73]. A primary antibody specific to the His₆-tag, namely the Anti-His₆ antibody [mouse] (Thermo Scientific), was used, along with a secondary antibody conjugated with horseradish peroxidase (HRP) (Anti-Mouse IgG-HRP [goat] (Thermo Scientific)) according to the manufacturer's instructions. Protein bands were detected using the 'SuperSignal™ West Femto Maximum Sensitivity Substrate' and visualized using the iBright FL1000 device (both from Thermo Scientific).

Expression and purification of recombinant PQO

The expression plasmid pET-28a-TEV/PQO was generated by Genscript (Leiden, The Netherlands), by synthesizing a DNA construct coding for PQO from *C. glutamicum* CS176 (GenBank accession no. WP_077313205), codon-optimized for protein expression in *E. coli* through

proprietary protocols and including a sequence coding for the TEV cleavage site (ENLYFQG) adjacent to the PQO initiator methionine. The construct was then inserted into the pET-28a *NdeI/XhoI* restriction sites. The resulting pET-28a-TEV-*pqo* plasmid was introduced into *E. coli* BL21 (DE3), and protein expression achieved in a 2YT-based autoinduction medium [74] supplemented with 50 µg kanamycin·mL⁻¹, through an initial 4 h growth step at 37 °C followed by overnight incubation at 18 °C. Cell pellets, stored at -80 °C, were resuspended in lysis buffer (25 mM Tris pH 8.5, 300 mM NaCl, 25 mM imidazole), freshly supplemented with benzonase and an IMAC compatible protease inhibitor cocktail (Roche, Mannheim, Germany) at 4 °C, and lysed by a CF2 cell disruptor (Constant Systems Ltd., Daventry, UK). The lysate was centrifuged for 1 h at 13 000 *g* at 4 °C, and the supernatant was loaded onto a 5 mL HisTrap FF crude Ni²⁺-IMAC column (Cytiva). Bound proteins were eluted with a linear gradient of IMAC elution buffer (25 mM Tris pH 8.5, 300 mM NaCl, 400 mM imidazole), and eluted fractions containing His₆-tagged PQO, as confirmed by SDS/PAGE, were pooled and supplemented with 1 mM DTT and TEV protease at a 1 : 30 (w/w) ratio, purified as described before [75]. The sample was then dialyzed overnight at 4 °C against 20 mM MES-NaOH pH 6.5, 50 mM NaCl, 10% glycerol using a 'SnakeSkin' dialysis tubing with a 7 kDa MW cut-off (ThermoFisher). Residual cleavage products as well as the TEV protease were then removed by passing the sample through a Ni-NTA agarose resin (Qiagen, Hilden, Germany) on a gravity-flow disposable 10 mL plastic column. The PQO containing flow-through was checked on SDS/PAGE, concentrated through a 10 kDa cut-off Vivaspin 20 device (Sartorius), and loaded onto a HiLoad 26/60 Superdex 200 size exclusion column (Cytiva), pre-equilibrated in 20 mM MES-NaOH pH 6.5, 50 mM NaCl, 10% glycerol. Fractions corresponding to the PQO peak were checked on SDS/PAGE, pooled and concentrated; the final PQO solution was aliquoted, flash-frozen in liquid nitrogen and stored at -80 °C.

Crystallization

Crystallization screenings were performed at 18 °C by vapor diffusion in 96-well plates ('sitting drop' method), following established protocols [76]. Natively purified PQO (from cells grown in acetate minimal media) crystallized at 7.5 mg·mL⁻¹ in 22% (w/v) PEG 4000, 0.2 M (NH₄)₂SO₄, 0.1 M sodium acetate. Recombinant PQO purified from *E. coli* crystallized at the concentration of 18 mg·mL⁻¹, following supplementation with 2 mM FAD, in 25% (w/v) PEG 4000, 8% (v/v) isopropanol, 0.1 M sodium acetate; crystals of the enzyme in complex with FAD and ThDP-Mg²⁺ were grown from the same concentrated protein solution supplemented with 2 mM FAD, 2 mM ThDP, 5 mM MgCl₂, and were obtained in 1.6 M tri-sodium citrate, pH

6.5. Crystals of PQO-Δ_{C17} were obtained from a 16 mg·mL⁻¹ purified protein solution, supplemented with 2 mM ThDP, 5 mM MgCl₂, in 35% methylpentanediol (MPD). Prior to be flash-frozen in liquid nitrogen, single crystals were soaked in a cryoprotectant solution made of either 50% Paratone-N (Hampton Research, Aliso Viejo, CA, USA) and 50% paraffine oil (in the case of full-length PQO and PQO-Δ_{C17} crystals), or 75% crystallization solution, 25% glycerol (crystals of recombinant PQO).

X-ray diffraction data collection and structure solution

Diffraction datasets were acquired on the beamlines ID23-1, ID30A-1, ID30A-3 at the ESRF synchrotron (Grenoble, France), or on the beamline Proxima-2A at SOLEIL (Saint-Aubin, France). Data integration and scaling were performed with *autoPROC* [47], applying anisotropic scaling via *STARANISO*. The PQO structure was initially solved by molecular replacement through the program *PHASER* [77], using the coordinates of proteolytically activated *E. coli* PoxB (PDB: 3EYA) as the search model, followed by automated model rebuilding with *ARP/wARP* [78]. Further steps of model modifications, including corrections and placement of solvent and cofactors in electron density maps were performed with *COOT* [79], alternated with refinement with *BUSTER* (Global Phasing Ltd.). Local structure similarity restraints for non-crystallographic symmetry (NCS) [80], as well as a Translation-Libration-Screw (TLS) model were applied where appropriate. Chemical dictionaries for ligands were generated with the Grade server (<http://grade.globalphasing.org>). Models were validated with *MOLPROBITY* [48] and the dedicated validation tools in *PHENIX* [81]. All structural figures were prepared with the software *PYMOLE* (The PyMOL Molecular Graphics System, version 3.0, Schrödinger, New York, NY, USA, LLC.). Data collection, refinement and model statistics are indicated in Table 3.

Acknowledgements

This work was funded by the ANR-DFG project METACTINO (ANR-18-CE92-0003; DFG Ei 561/5-1), and by institutional funds from the Institut Pasteur, the CNRS and the Université Paris Cité. We are grateful to E.M. Bruch and A. Boyko for their initial work on PQO expression and crystallization, and to the Institut Pasteur Crystallography Platform (part of the Centre for Technological Resources and Research) and its staff, namely to P. Weber and C. Pissis for performing crystallization screenings. We also thank the synchrotron sources ESRF and Soleil for providing access to their facilities, and their respective staff for helpful assistance on the beamlines. LY was a student

of the Pasteur – Paris University (PPU) International PhD program and was supported by the Wuhan Institute of Biological Products Co. Ltd. (Wuhan, People's Republic of China), a subsidiary company of China National Biotech Group Company Limited, and by a doctoral fellowship from the China Scholarship Council (CSC).

Conflict of interest

The authors declare no conflict of interest.

Author contributions

CSL performed the ensemble of the *C. glutamicum* growth and phenotype analysis experiments, purified PQO from *C. glutamicum* and performed activity assays; SM performed the continuous cultivation experiments; LY expressed and purified recombinant PQO; MB collected and processed X-ray diffraction data, refined and analyzed the atomic models; BJE supervised the work; CSL, BJE and MB wrote the paper; all authors agreed on the manuscript content.

Peer review

The peer review history for this article is available at <https://www.webofscience.com/api/gateway/wos/peer-review/10.1111/febs.17232>.

Data availability statement

Coordinates, structure factors and validation reports supporting these findings are openly available in the wwPDB at <https://doi.org/10.2210/pdb9EV3/pdb> (PQO purified from *C. glutamicum* ATCC13032 cells grown in acetate minimal medium), <https://doi.org/10.2210/pdb9EV4/pdb> (recombinant *C. glutamicum* CS176 PQO expressed in *E. coli*), <https://doi.org/10.2210/pdb9EV5/pdb> (recombinant *C. glutamicum* CS176 PQO expressed in *E. coli* and co-crystallized with ThDP and Mg²⁺), <https://doi.org/10.2210/pdb9EV6/pdb> (PQO- Δ_{C17} co-crystallized with ThDP and Mg²⁺).

References

- 1 Liebl W (2006) *Corynebacterium* – nonmedical. In The Prokaryotes (Dworkin M, Falkow S, Rosenberg E, Schleifer KH & Stackebrandt E, eds), pp. 796–818. Springer, New York, NY.
- 2 Abe S, Takayama K-I & Kinoshita S (1967) Taxonomical studies on glutamic acid-producing bacteria. *J Gen Appl Microbiol* **13**, 279–301.
- 3 Eggeling L & Bott M (2015) A giant market and a powerful metabolism: L-lysine provided by *Corynebacterium glutamicum*. *Appl Microbiol Biotechnol* **99**, 3387–3394.
- 4 Wendisch VF (2020) Metabolic engineering advances and prospects for amino acid production. *Metab Eng* **58**, 17–34.
- 5 Becker J, Rohles CM & Wittmann C (2018) Metabolically engineered *Corynebacterium glutamicum* for bio-based production of chemicals, fuels, materials, and healthcare products. *Metab Eng* **50**, 122–141.
- 6 Wolf S, Becker J, Tsuge Y, Kawaguchi H, Kondo A, Marienhagen J, Bott M, Wendisch VF & Wittmann C (2021) Advances in metabolic engineering of *Corynebacterium glutamicum* to produce high-value active ingredients for food, feed, human health, and well-being. *Essays Biochem* **65**, 197–212.
- 7 Cocaign M, Monnet C & Lindley ND (1993) Batch kinetics of *Corynebacterium glutamicum* during growth on various carbon substrates: use of substrate mixtures to localise metabolic bottlenecks. *Appl Microbiol Biotechnol* **40**, 526–530.
- 8 Wendisch VF, de Graaf AA, Sahn H & Eikmanns BJ (2000) Quantitative determination of metabolic fluxes during Coutilization of two carbon sources: comparative analyses with *Corynebacterium glutamicum* during growth on acetate and/or glucose. *J Bacteriol* **182**, 3088–3096.
- 9 Blombach B & Seibold GM (2010) Carbohydrate metabolism in *Corynebacterium glutamicum* and applications for the metabolic engineering of L-lysine production strains. *Appl Microbiol Biotechnol* **86**, 1313–1322.
- 10 Leßmeier L, Matano C, Zahoor A, Lindner SN & Wendisch VF (2015) Metabolic engineering of *Corynebacterium glutamicum* for alternative carbon source utilization. In *Corynebacterium glutamicum: From Systems Biology to Biotechnological Applications* (Burkovski A, ed.), pp. 57–70. Caister Academic Press, Wymondham, UK.
- 11 Kogure T & Inui M (2018) Recent advances in metabolic engineering of *Corynebacterium glutamicum* for bioproduction of value-added aromatic chemicals and natural products. *Appl Microbiol Biotechnol* **102**, 8685–8705.
- 12 Yokota A & Lindley ND (2005) Central metabolism: sugar uptake and conversion. In *Handbook of Corynebacterium glutamicum* (Eggeling L & Bott M, eds), pp. 215–240. CRC, Boca Raton, FL.
- 13 Eikmanns BJ (2005) Central metabolism: tricarboxylic acid cycle and anaplerotic reactions. In *Handbook of Corynebacterium glutamicum* (Eggeling L & Bott M, eds), pp. 241–276. CRC, Boca Raton, FL.
- 14 Sauer U & Eikmanns BJ (2005) The PEP—pyruvate—oxaloacetate node as the switch point for carbon flux

- distribution in bacteria. *FEMS Microbiol Rev* **29**, 765–794.
- 15 Arndt A & Eikmanns BJ (2008) Regulation of carbon metabolism in *Corynebacterium glutamicum*. In *Corynebacteria: Genomics and Molecular Biology* (Burkovski A, ed.), pp. 155–182. Horizon Scientific press, Norwich, UK.
- 16 Bott M & Eikmanns BJ (2013) TCA cycle and glyoxylate shunt of *Corynebacterium glutamicum*. In *Corynebacterium glutamicum: Biology and Biotechnology* (Yukawa H & Inui M, eds), pp. 281–313. Springer, Berlin, Heidelberg.
- 17 Schreiner ME, Fiur D, Holátko J, Pátek M & Eikmanns BJ (2005) E1 enzyme of the pyruvate dehydrogenase complex in *Corynebacterium glutamicum*: molecular analysis of the gene and Phylogenetic aspects. *J Bacteriol* **187**, 6005–6018.
- 18 Buchholz J, Schwentner A, Brunnenkan B, Gabris C, Grimm S, Gerstmeir R, Takors R, Eikmanns BJ & Blombach B (2013) Platform engineering of *Corynebacterium glutamicum* with reduced pyruvate dehydrogenase complex activity for improved production of L-lysine, L-valine, and 2-Ketoisovalerate. *Appl Environ Microbiol* **79**, 5566–5575.
- 19 Eikmanns BJ & Blombach B (2014) The pyruvate dehydrogenase complex of *Corynebacterium glutamicum*: an attractive target for metabolic engineering. *J Biotechnol* **192**, 339–345.
- 20 Niebisch A, Kabus A, Schultz C, Weil B & Bott M (2006) Corynebacterial protein kinase G controls 2-oxoglutarate dehydrogenase activity via the phosphorylation status of the OdhI protein. *J Biol Chem* **281**, 12300–12307.
- 21 Hoffelder M, Raasch K, van Ooyen J & Eggeling L (2010) The E2 domain of OdhA of *Corynebacterium glutamicum* has succinyltransferase activity dependent on Lipoyl residues of the acetyltransferase AceF. *J Bacteriol* **192**, 5203–5211.
- 22 Kinugawa H, Kondo N, Komine-Abe A, Tomita T, Nishiyama M & Kosono S (2020) *In vitro* reconstitution and characterization of pyruvate dehydrogenase and 2-oxoglutarate dehydrogenase hybrid complex from *Corynebacterium glutamicum*. *Microbiologyopen* **9**, e1113.
- 23 Bruch EM, Vilela P, Yang L, Boyko A, Lexa-Sapart N, Raynal B, Alzari PM & Bellinzoni M (2021) Actinobacteria challenge the paradigm: a unique protein architecture for a well-known, central metabolic complex. *Proc Natl Acad Sci USA* **118**, e2112107118.
- 24 Yang L, Wagner T, Mechaly A, Boyko A, Bruch EM, Megrian D, Gubellini F, Alzari PM & Bellinzoni M (2023) High resolution cryo-EM and crystallographic snapshots of the actinobacterial two-in-one 2-oxoglutarate dehydrogenase. *Nat Commun* **14**, 4851.
- 25 Sundermeyer L, Folkerts J-G, Lückel B, Mack C, Baumgart M & Bott M (2023) Cellular localization of the hybrid pyruvate/2-oxoglutarate dehydrogenase complex in the actinobacterium *Corynebacterium glutamicum*. *Microbiol Spectr* **11**, e0266823.
- 26 Schreiner ME & Eikmanns BJ (2005) Pyruvate:quinone oxidoreductase from *Corynebacterium glutamicum*: purification and biochemical characterization. *J Bacteriol* **187**, 862–871.
- 27 Sousa FM, Fernandes B & Pereira MM (2023) The protein family of pyruvate:quinone oxidoreductases: amino acid sequence conservation and taxonomic distribution. *Biochim Biophys Acta Bioenerg* **1864**, 148958.
- 28 Schreiner ME, Riedel C, Holátko J, Pátek M & Eikmanns BJ (2006) Pyruvate:quinone oxidoreductase in *Corynebacterium glutamicum*: molecular analysis of the *pqo* gene, significance of the enzyme, and phylogenetic aspects. *J Bacteriol* **188**, 1341–1350.
- 29 Hager LP (1957) Trypsin activation of a ferricyanide-linked pyruvic acid oxidation. *J Biol Chem* **229**, 251–263.
- 30 Chang YY & Cronan JE (1983) Genetic and biochemical analyses of *Escherichia coli* strains having a mutation in the structural gene (*poxB*) for pyruvate oxidase. *J Bacteriol* **154**, 756–762.
- 31 Koland JG, Miller MJ & Gennis RB (1984) Reconstitution of the membrane-bound, ubiquinone-dependent pyruvate oxidase respiratory chain of *Escherichia coli* with the cytochrome d terminal oxidase. *Biochemistry* **23**, 445–453.
- 32 Carter K & Gennis RB (1985) Reconstitution of the ubiquinone-dependent pyruvate oxidase system of *Escherichia coli* with the cytochrome o terminal oxidase complex. *J Biol Chem* **260**, 10986–10990.
- 33 Marchal D, Pantigny J, Laval JM, Moiroux J & Bourdillon C (2001) Rate constants in two dimensions of electron transfer between pyruvate oxidase, a membrane enzyme, and ubiquinone (coenzyme Q8), its water-insoluble electron carrier. *Biochemistry* **40**, 1248–1256.
- 34 Hager LP, Geller DM & Lipmann F (1954) Flavoprotein-catalyzed pyruvate oxidation in *Lactobacillus delbrueckii*. *Fed Proc* **13**, 734–738.
- 35 Muller YA & Schulz GE (1993) Structure of the thiamine- and flavin-dependent enzyme pyruvate oxidase. *Science* **259**, 965–967.
- 36 Sedewitz B, Schleifer KH & Götz F (1984) Purification and biochemical characterization of pyruvate oxidase from *Lactobacillus plantarum*. *J Bacteriol* **160**, 273–278.
- 37 Tittmann K, Golbik R, Ghisla S & Hübner G (2000) Mechanism of elementary catalytic steps of pyruvate oxidase from *Lactobacillus plantarum*. *Biochemistry* **39**, 10747–10754.

- 38 Cunningham CC & Hager LP (1971) Crystalline pyruvate oxidase from *Escherichia coli*: II. Activation by phospholipids. *J Biol Chem* **246**, 1575–1582.
- 39 Cunningham CC & Hager LP (1971) Crystalline pyruvate oxidase from *Escherichia coli*: III. Phospholipid as an allosteric effector for the enzyme. *J Biol Chem* **246**, 1583–1589.
- 40 Cunningham CC & Hager LP (1975) Reactivation of the lipid-depleted pyruvate oxidase system from *Escherichia coli* with cell envelope neutral lipids. *J Biol Chem* **250**, 7139–7146.
- 41 Russell P, Hager LP & Gennis RB (1977) Characterization of the proteolytic activation of pyruvate oxidase. Control by specific ligands and by the flavin oxidation-reduction state. *J Biol Chem* **252**, 7877–7882.
- 42 Blake R, O'Brien TA, Gennis RB & Hager LP (1982) Role of the divalent metal cation in the pyruvate oxidase reaction. *J Biol Chem* **257**, 9605–9611.
- 43 Recny MA, Grabau C, Cronan JE & Hager LP (1985) Characterization of the alpha-peptide released upon protease activation of pyruvate oxidase. *J Biol Chem* **260**, 14287–14291.
- 44 Wang AY, Chang YY & Cronan JE (1991) Role of the tetrameric structure of *Escherichia coli* pyruvate oxidase in enzyme activation and lipid binding. *J Biol Chem* **266**, 10959–10966.
- 45 Weidner A, Neumann P, Pech A, Stubbs MT & Tittmann K (2009) New insights into the membrane-binding and activation mechanism of pyruvate oxidase from *Escherichia coli*. *J Mol Catal B Enzym* **61**, 88–92.
- 46 Neumann P, Weidner A, Pech A, Stubbs MT & Tittmann K (2008) Structural basis for membrane binding and catalytic activation of the peripheral membrane enzyme pyruvate oxidase from *Escherichia coli*. *Proc Natl Acad Sci USA* **105**, 17390–17395.
- 47 Vonrhein C, Flensburg C, Keller P, Sharff A, Smart O, Paciorek W, Womack T & Bricogne G (2011) Data processing and analysis with the autoPROC toolbox. *Acta Cryst D* **67**, 293–302.
- 48 Williams CJ, Headd JJ, Moriarty NW, Prisant MG, Videau LL, Deis LN, Verma V, Keedy DA, Hintze BJ, Chen VB *et al.* (2018) MolProbity: more and better reference data for improved all-atom structure validation. *Protein Sci* **27**, 293–315.
- 49 Wille G, Ritter M, Weiss MS, König S, Mäntele W & Hübner G (2005) The role of Val-265 for flavin adenine dinucleotide (FAD) binding in pyruvate oxidase: FTIR, kinetic, and crystallographic studies on the enzyme variant V265A. *Biochemistry* **44**, 5086–5094.
- 50 Abdel-Hamid AM, Attwood MM & Guest JR (2001) Pyruvate oxidase contributes to the aerobic growth efficiency of *Escherichia coli*. *Microbiology (Reading)* **147**, 1483–1498.
- 51 Li M, Yao S & Shimizu K (2007) Effect of *poxB* gene knockout on metabolism in *Escherichia coli* based on growth characteristics and enzyme activities. *World J Microbiol Biotechnol* **23**, 573–580.
- 52 Moreau PL (2004) Diversion of the metabolic flux from pyruvate dehydrogenase to pyruvate oxidase decreases oxidative stress during glucose metabolism in nongrowing *Escherichia coli* cells incubated under aerobic, phosphate starvation conditions. *J Bacteriol* **186**, 7364–7368.
- 53 Petersen S, Mack C, de Graaf AA, Riedel C, Eikmanns BJ & Sahm H (2001) Metabolic consequences of altered phosphoenolpyruvate carboxykinase activity in *Corynebacterium glutamicum* reveal anaplerotic regulation mechanisms *in vivo*. *Metab Eng* **3**, 344–361.
- 54 Blombach B, Schreiner ME, Moch M, Oldiges M & Eikmanns BJ (2007) Effect of pyruvate dehydrogenase complex deficiency on L-lysine production with *Corynebacterium glutamicum*. *Appl Microbiol Biotechnol* **76**, 615–623.
- 55 Blombach B, Schreiner ME, Bartek T, Oldiges M & Eikmanns BJ (2008) *Corynebacterium glutamicum* tailored for high-yield L-valine production. *Appl Microbiol Biotechnol* **79**, 471–479.
- 56 Krause FS, Blombach B & Eikmanns BJ (2010) Metabolic engineering of *Corynebacterium glutamicum* for 2-ketoisovalerate production. *Appl Environ Microbiol* **76**, 8053–8061.
- 57 Blombach B, Riestler T, Wieschalka S, Ziert C, Youn J-W, Wendisch VF & Eikmanns BJ (2011) *Corynebacterium glutamicum* tailored for efficient Isobutanol production. *Appl Environ Microbiol* **77**, 3300–3310.
- 58 Krug A, Wendisch VF & Bott M (2005) Identification of AcnR, a TetR-type repressor of the aconitase gene *acn* in *Corynebacterium glutamicum*. *J Biol Chem* **280**, 585–595.
- 59 Molenaar D, van der Rest ME, Drysch A & Yücel R (2000) Functions of the membrane-associated and cytoplasmic malate dehydrogenases in the citric acid cycle of *Corynebacterium glutamicum*. *J Bacteriol* **182**, 6884–6891.
- 60 Gerstmeier R, Wendisch VF, Schnicke S, Ruan H, Farwick M, Reinscheid D & Eikmanns BJ (2003) Acetate metabolism and its regulation in *Corynebacterium glutamicum*. *J Biotechnol* **104**, 99–122.
- 61 Graf M, Haas T, Teleki A, Feith A, Cerff M, Wiechert W, Nöh K, Busche T, Kalinowski J & Takors R (2020) Revisiting the growth Modulon of *Corynebacterium glutamicum* under glucose limited chemostat conditions. *Front Bioeng Biotechnol* **8**, 584614.
- 62 Bendt AK, Burkovski A, Schaffer S, Bott M, Farwick M & Hermann T (2003) Towards a phosphoproteome map of *Corynebacterium glutamicum*. *Proteomics* **3**, 1637–1646.

- 63 Mizuno Y, Nagano-Shoji M, Kubo S, Kawamura Y, Yoshida A, Kawasaki H, Nishiyama M, Yoshida M & Kosono S (2016) Altered acetylation and succinylation profiles in *Corynebacterium glutamicum* in response to conditions inducing glutamate overproduction. *Microbiologyopen* **5**, 152–173.
- 64 Küberl A, Fränzel B, Eggeling L, Polen T, Wolters DA & Bott M (2014) Pupylated proteins in *Corynebacterium glutamicum* revealed by MudPIT analysis. *Proteomics* **14**, 1531–1542.
- 65 Küberl A, Polen T & Bott M (2016) The pupylation machinery is involved in iron homeostasis by targeting the iron storage protein ferritin. *Proc Natl Acad Sci USA* **113**, 4806–4811.
- 66 Huc E, Meniche X, Benz R, Bayan N, Ghazi A, Tropis M & Daffé M (2010) O-Mycoloylated proteins from *Corynebacterium*: an unprecedented post-translational modification in bacteria. *J Biol Chem* **285**, 21908–21912.
- 67 Komine-Abe A, Kondo N, Kubo S, Kawasaki H, Nishiyama M & Kosono S (2021) Characterization of lysine acetylation in the peripheral subunit-binding domain of the E2 subunit of the pyruvate dehydrogenase-2-oxoglutarate dehydrogenase hybrid complex from *Corynebacterium glutamicum*. *Biosci Biotechnol Biochem* **85**, 874–881.
- 68 Nagano-Shoji M, Hamamoto Y, Mizuno Y, Yamada A, Kikuchi M, Shirouzu M, Umehara T, Yoshida M, Nishiyama M & Kosono S (2017) Characterization of lysine acetylation of a phosphoenolpyruvate carboxylase involved in glutamate overproduction in *Corynebacterium glutamicum*. *Mol Microbiol* **104**, 677–689.
- 69 Jumper J, Evans R, Pritzel A, Green T, Figurnov M, Ronneberger O, Tunyasuvunakool K, Bates R, Žídek A, Potapenko A *et al.* (2021) Highly accurate protein structure prediction with AlphaFold. *Nature* **596**, 583–589.
- 70 Eikmanns BJ, Metzger M, Reinscheid D, Kircher M & Sahm H (1991) Amplification of three threonine biosynthesis genes in *Corynebacterium glutamicum* and its influence on carbon flux in different strains. *Appl Microbiol Biotechnol* **34**, 617–622.
- 71 Liebl W, Bayerl A, Schein B, Stillner U & Schleifer KH (1989) High efficiency electroporation of intact *Corynebacterium glutamicum* cells. *FEMS Microbiol Lett* **65**, 299–303.
- 72 Bordier C (1981) Phase separation of integral membrane proteins in triton X-114 solution. *J Biol Chem* **256**, 1604–1607.
- 73 Towbin H, Staehelin T & Gordon J (1979) Electrophoretic transfer of proteins from polyacrylamide gels to nitrocellulose sheets: procedure and some applications. *Proc Natl Acad Sci USA* **76**, 4350–4354.
- 74 Studier FW (2005) Protein production by auto-induction in high density shaking cultures. *Protein Expr Purif* **41**, 207–234.
- 75 van den Berg S, Löfdahl P-Å, Härd T & Berglund H (2006) Improved solubility of TEV protease by directed evolution. *J Biotechnol* **121**, 291–298.
- 76 Weber P, Pissis C, Navaza R, Mechaly AE, Saul F, Alzari PM & Haouz A (2019) High-throughput crystallization pipeline at the crystallography Core Facility of the Institut Pasteur. *Molecules* **24**, 4451.
- 77 McCoy AJ, Grosse-Kunstleve RW, Adams PD, Winn MD, Storoni LC & Read RJ (2007) Phaser crystallographic software. *J Appl Crystallogr* **40**, 658–674.
- 78 Cohen SX, Ben Jelloul M, Long F, Vagin A, Knipscheer P, Lebbink J, Sixma TK, Lamzin VS, Murshudov GN & Perrakis A (2008) ARP/wARP and molecular replacement: the next generation. *Acta Cryst D* **64**, 49–60.
- 79 Emsley P, Lohkamp B, Scott WG & Cowtan K (2010) Features and development of Coot. *Acta Cryst D* **66**, 486–501.
- 80 Smart OS, Womack TO, Flensburg C, Keller P, Paciorek W, Sharff A, Vornrhein C & Bricogne G (2012) Exploiting structure similarity in refinement: automated NCS and target-structure restraints in BUSTER. *Acta Cryst D* **68**, 368–380.
- 81 Liebschner D, Afonine PV, Baker ML, Bunkóczi G, Chen VB, Croll TI, Hintze B, Hung LW, Jain S, McCoy AJ *et al.* (2019) Macromolecular structure determination using X-rays, neutrons and electrons: recent developments in Phenix. *Acta Cryst D* **75**, 861–877.

Supporting information

Additional supporting information may be found online in the Supporting Information section at the end of the article.

Fig. S1. Representative UV–visible spectra of PQQ preparations.

Fig. S2. Overview of the *C. glutamicum* PQQ monomer in complex with FAD and ThDP, and comparison with *E. coli* PoxB.

Fig. S3. Electron density for bound FAD in the highest resolution PQQ model, and observed bending of the isoalloxanic FAD moiety.

Fig. S4. Sequence alignment of PQQ from *C. glutamicum* ATCC13032 and representative homologous sequences from the PQQ/pyruvate oxidase family.

Fig. S5. Cartoon representation and properties of the *C. glutamicum* PQQ C-terminal helix.

Fig. S6. Comparison of PQQ monomer models obtained from crystals of recombinant *C. glutamicum* PQQ expressed in *E. coli*, with and without bound ThDP.

Fig. S7. Comparison of PQQ- Δ_{C17} and full-length PQQ monomer models.

Fig. S8. Superimposition of *C. glutamicum* PQQ models in ternary complex with FAD and ThDP to *E. coli* PoxB, in either full-length form or following proteolytic activation.

Fig. S9. AlphaFold2 model of *C. glutamicum* PQQ and main differences with respect to the highest resolution experimental model.

Table S1. Bacterial strains and plasmids used in this study.

Table S2. Oligonucleotides used in this study.